

Report on Consistent MERRA – Atmospheric Trace Gas Distributions

Sarah Strode and Zhengxin Zhu

I. Introduction

The global distribution of atmospheric trace gases has important consequences for air quality and human health as well as climate and radiation. The wealth of ground-based, aircraft, and satellite data for the first decade of the 21st century provides valuable constraints on the temporal and geographic distribution of trace gases. Inter-annual variability in trace gas concentrations is driven by year-to-year changes in meteorology as well as natural and anthropogenic emissions.

This project seeks to simulate the global distribution and temporal variability of atmospheric trace gases in recent years using a consistent set of meteorology and emissions. We describe several milestones achieved in developing consistent trace gas distributions. These include the development and testing of trace gas emissions, an examination of the impact of horizontal resolution, and model validation against observations. We also describe preliminary results of the replay simulation.

Trace gases including CO, ozone, NO_x, hydrocarbons, and halocarbons are simulated using the GEOS-CCMv3. The GEOS-CCMv3 includes GMI stratospheric (*Strahan et al.*, 2007) and tropospheric chemistry (*Duncan et al.*, 2007a) within GEOS5 (*Rienecker et al.*, 2008). Either the MERRA meteorological analysis for specific years or the free-running GCM can drive the online tracer transport in the model.

II. Emissions specification

Emissions of CO and other ozone precursors vary from year to year due to changes in anthropogenic activities and interannual variability in natural emissions and biomass burning. Our simulation includes year-specific emissions of CO, NO_x, and NMHCs to account for the impact of emission variability on the variability of trace gas concentrations. Long-lived gases such as methane, N₂O, and CFCs are treated as surface boundary conditions. Biogenic emissions of isoprene, monoterpene, and methyl butanol are calculated online based on the MEGAN inventory (*Guenther et al.*, 1995; *Guenther et al.*, 1999; *Guenther and Wiedenmeier*, 2004).

This section focuses on the development of year-specific emissions for CO, NO_x, and NMHCs from fossil fuels, biofuels, and biomass burning. We developed these emissions based on routines and inventory data sets provided by the Harvard University GEOS-Chem group. We implement the routines offline to create emission fields and then read the emission field for a

given year into the model. We begin with a global inventory for fossil fuels and biofuels and overwrite particular regions with regional inventory data where it is available. Since anthropogenic inventories typically represent a single year, fossil fuel emissions are scaled from the inventory base year to the simulation year using scaling factors from the Harvard University GEOS-Chem group (*van Donkelaar et al.*, 2008). The strength and distribution of biomass burning emissions are constrained by satellite data. We use emission factors for boreal forest, tropical forest, and savanna/herb/other vegetation types to convert GFED2 (*Randerson et al.*, 2007; *Van der Werf et al.*, 2006) carbon emissions to emissions of NO_x, CO, or VOCs. The emissions of individual sources are described in the GEOS5 Wiki (http://geos5.org/wiki/index.php?title=GEOS-5_GMI_Configuration_for_PIESA) and below.

NO_x sources

- Aircraft NO_x: Steven Baughcum provided aircraft emissions of NO_x for 1995 on a 1x1 degree grid with 1 km vertical resolution. We then vertically regridded the aircraft data to the GEOS5 72-level vertical grid.
- Climatological lightning NO_x
- Global NO_x emissions from fossil fuels are from the EDGAR inventory for 2000. The following regional inventories then overwrite the global inventory:
 - EPA/NEI 2005 over the United States, with seasonality from the VISTAS inventory
 - CAC 2002 and 2005 over Canada: 2002 for years 2002 and earlier, 2005 for years 2005 and later, and interpolated between the 2002 and 2005 inventory for 2003 and 2004
 - BRAVO over northern Mexico
 - year-specific EMEP over Europe
 - *Streets et al.* (2003) inventory for 2000 with seasonality from the 2004 inventory over southeast Asia for years prior to 2006; *Zhang et al.* (2009) inventory for 2006 over southeast Asia for 2006 and later
- Ship emissions of NO_x are omitted, as described later in this section
- Global biofuel NO_x emissions are from *Yevich et al.* (2003). These are overwritten with EPA/NEI 1999 biofuels over the United States. For years 2006 and later, biofuel emissions are zeroed over southeast Asia to avoid double counting because the 2006 inventory for southeast Asia does not separate fossil fuels and biofuels.
- NO_x is emitted as NO.

CO sources

- Global CO emissions from fossil fuels are from the EDGAR inventory for 2000. We impose a

seasonal cycle north of 36 degrees N (except over China, where the inventory is already monthly) with emissions 10% higher during winter and 10% lower during summer, following *Duncan et al.* (2007b).

- The following regional inventories overwrite the global inventory for fossil fuel CO:
 - EPA/NEI 2005 over the United States, with seasonality from the EPA/NEI 1999 inventory
 - CAC 2002 and 2005 over Canada: 2002 for years 2002 and earlier, 2005 for years 2005 and later, and interpolated between the 2002 and 2005 inventory for 2003 and 2004
 - BRAVO over northern Mexico
 - year-specific EMEP over Europe
 - Years up through 2005: *Streets et al.* (2003) inventory for 2000 over southeast Asia, overwritten with *Streets et al.* (2006) inventory for 2001 over China. For 2006 and later, *Zhang et al.* (2009) inventory for 2006 over southeast Asia.
- Global biofuel CO emissions are from *Yevich et al.* (2003). These are overwritten with EPA/NEI 1999 biofuels over the United States. For years 2006 and later, biofuel emissions are zeroed over southeast Asia to avoid double counting because the 2006 inventory for southeast Asia does not separate fossil fuels and biofuels.
- To account for CO production from co-emitted non-methane hydrocarbons, we scale up fossil fuel CO emissions by 2%, biofuel CO emissions by 8.6%, and biomass burning CO emissions by 5%.

VOC sources

- Global fossil fuel emissions of MEK, PRPE, C₂H₆, C₃H₈, and ALK₄ come from GEOS-Chem's inventory for 1985 (*Wang et al.* 1998), based on speciation information from EPA. Annual scaling of VOC's uses the same scaling factors as CO.
- The following regional inventories overwrite the global VOC emissions:
 - EPA/NEI 2005 over the United States for all species, with seasonality from EPA/NEI 1999
 - EMEP over Europe for MEK, PRPE, C₂H₆, and ALK₄
 - For 2006 and later, *Zhang et al.* (2009) inventory for 2006 over southeast Asia
- Biofuel emissions of MEK, PRPE, C₂H₆, C₃H₈, ALK₄, CH₂O, and ALD₂ come from *Yevich et al.* (2003). All species except CH₂O are overwritten with EPA/NEI1999 biofuels over the US. For years 2006 and later, biofuel emissions are zeroed over southeast Asia to avoid double counting because the 2006 inventory for southeast Asia does not separate fossil fuels and biofuels.

Impact of changing emissions on trace gas distributions

We quantified the impact of the 2000-2005 change in emissions using the free-running GCM, model version Fortuna 2.0. We ran two sets of simulation, one with emissions for 2000 and one with emissions for 2005. For each emission year, we ran the model for 5 years. The first 2 years are spin-up, and we averaged the results of the last 3 years to give an ensemble average representation for each emission year. Figure 1 shows the July surface concentrations of CO and NO_x for 2005, the difference in concentration between the 2000 and 2005 ensembles, and the difference in emissions. The change in surface concentration closely follows the pattern of emission changes. Interannual variability in biomass burning leads to greater concentrations of both species in South America and Alaska in 2005 compared to 2000. Increasing anthropogenic emissions drive increasing concentrations in East Asia, while emission reductions in the eastern United States lead to decreased concentrations there, especially for NO_x.

Figure 2 shows the July 2005 surface concentration of ozone, and the 2005-2000 concentration difference. Because CO and NO_x are important ozone precursors, the changes in ozone concentration show a similar pattern to the changes in CO and NO_x. However, the ozone changes are more complex because of the non-linearity of ozone chemistry, and because changes in trace gases such as ozone that are also greenhouse gases feedback on the meteorology in the free GCM.

Ship emissions of NO_x

Ships emit NO_x and other pollutants in plumes within the relatively clean marine atmosphere.

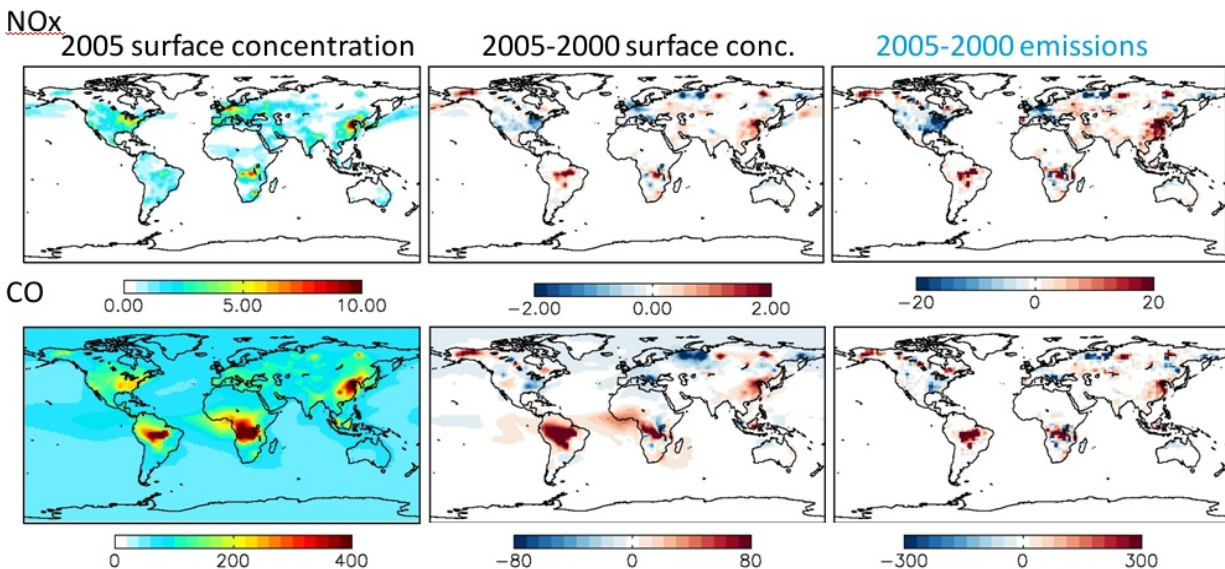


Figure 1. Left: July surface concentrations of NO_x and CO using 2005 emissions (ppbv). Center: Difference in surface concentrations between the ensemble with 2005 emissions and the ensemble with 2000 emissions (ppbv). Right: The difference in emissions between 2000 and 2005 (kg/m²/s).

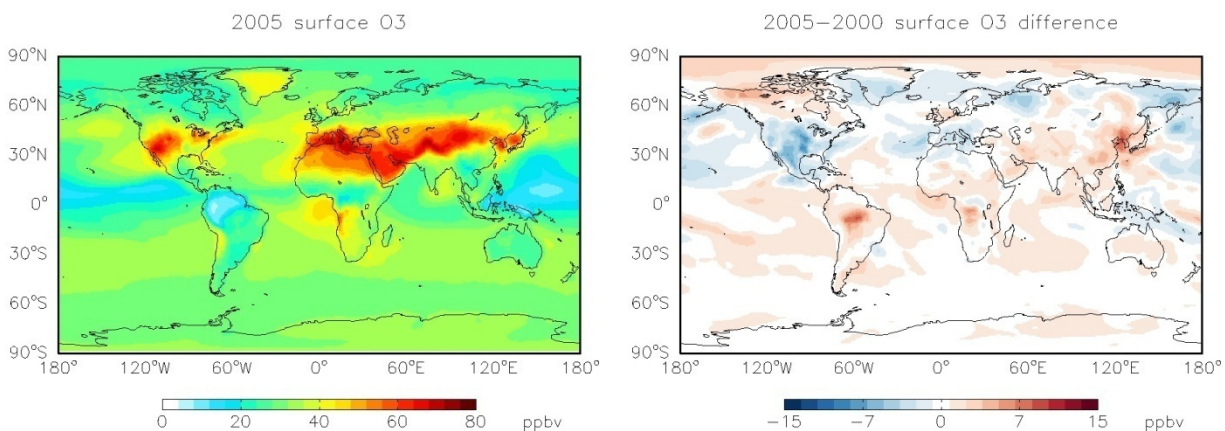


Figure 2. Left: July 2005 surface concentration of ozone. Right: Difference in July ozone surface concentration between 2005 and 2000.

Ship-plume chemistry is not well represented within the model, and the large size of the model grid boxes compared to the size of a ship plume leads to dilution of ship NO_x and hence an overestimate of the ozone production efficiency in regions with ship emissions. Previous studies have described the tendency of large-scale models to overestimate ozone production from ship emissions (*e.g.* Charlton-Perez *et al.* 2009). The simulations shown above, which included ship NO_x emissions, resulted in high ozone concentrations along ship tracks. High ozone along ship tracks resulted in high OH along the ship tracks, which in turn led to high chemical loss of CO. In comparison to the NOAA GMD observations (Novelli and Masarie, 2009), the model CO was biased low. This bias remained even when the model resolution was increased from 2×2.5 to 1×1.25 degree resolution. Consequently, we remove ship NO_x from the emissions used later in this study.

III. Impact of model resolution

The base simulations discussed in this report have a horizontal resolution of 2 degrees latitude by 2.5 degrees longitude. We also conducted a simulation at 1 degree latitude by 1.25 degrees longitude to examine the impact of increasing resolution. Here, we compare two GCM simulations using emissions for 2005, one with 2×2.5 degree resolution and one with 1×1.25 degree resolution. The emissions are input at the resolution of the simulation. Given the computational intensity of the 1×1.25 simulation, we compare a single year rather than an ensemble of years.

Figure 3 shows a comparison of surface CO concentration for September with the GMD CO observations (Novelli and Masarie, 2009) for the two model resolutions. The surface CO field looks qualitatively similar for both resolutions, but there is a small improvement in the statistical comparison to observations with the higher resolution. In particular, the excessive transport of South American biomass burning CO westward over the Pacific is less severe in the

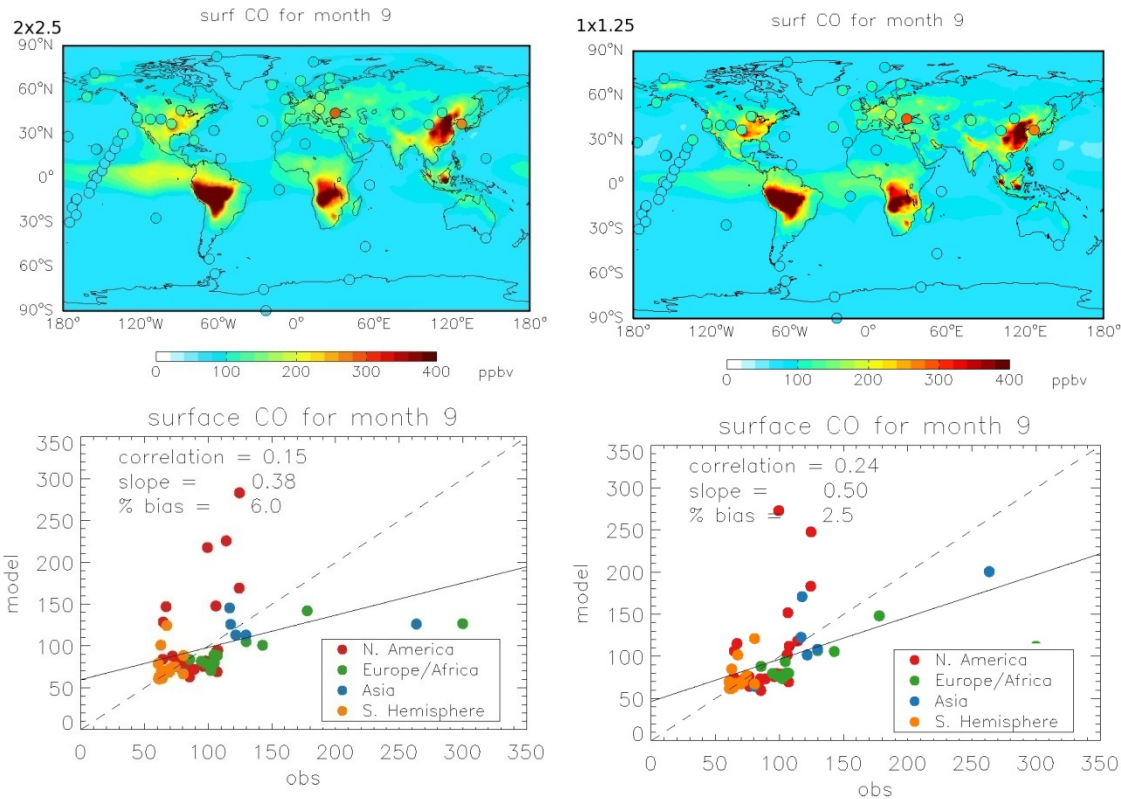


Figure 3. September surface CO concentration for the model at 2x2.5 degree resolution (left) and 1x1.25 degree resolution (right), with observations from the GMD network overplotted in circles. The bottom panels plot model concentrations versus the GMD observations

higher resolution simulation. However, an ensemble of more than one year would be useful for determining the robustness of this finding.

The INTEX-B campaign (*Singh et al., 2009*) took place in spring of 2006. Figures 4 and 5 compare the modeled vertical profiles of four constituents to observations from the DC8 aircraft during the Pacific phase of INTEX-B. The observations were obtained from the INTEX-B website (<http://www.espo.nasa.gov/intex-b/>). We sample daily means from the 2x2.5 degree resolution model (Figure 4) and the 1x1.25 degree resolution model (Figure 5) along the INTEX-B flight tracks and bin both the model (red) and the observations (black) by altitude into 1 km bins to obtain the mean and standard deviation for each altitude. We also bin the observations by model grid box (gray) to remove sub-grid-scale variability. All flights are considered together since the GCM will not capture the specific air masses sampled in each flight.

The model simulates ozone well below 7 km at both resolutions. At higher altitude, the variability increases, but the mean of the 1x1.25 degree model agrees slightly better with the observations. CO is underestimated throughout the column at both resolutions, likely due to the inclusion of ship emissions, as discussed in section II. Methane and NO_x are well-simulated

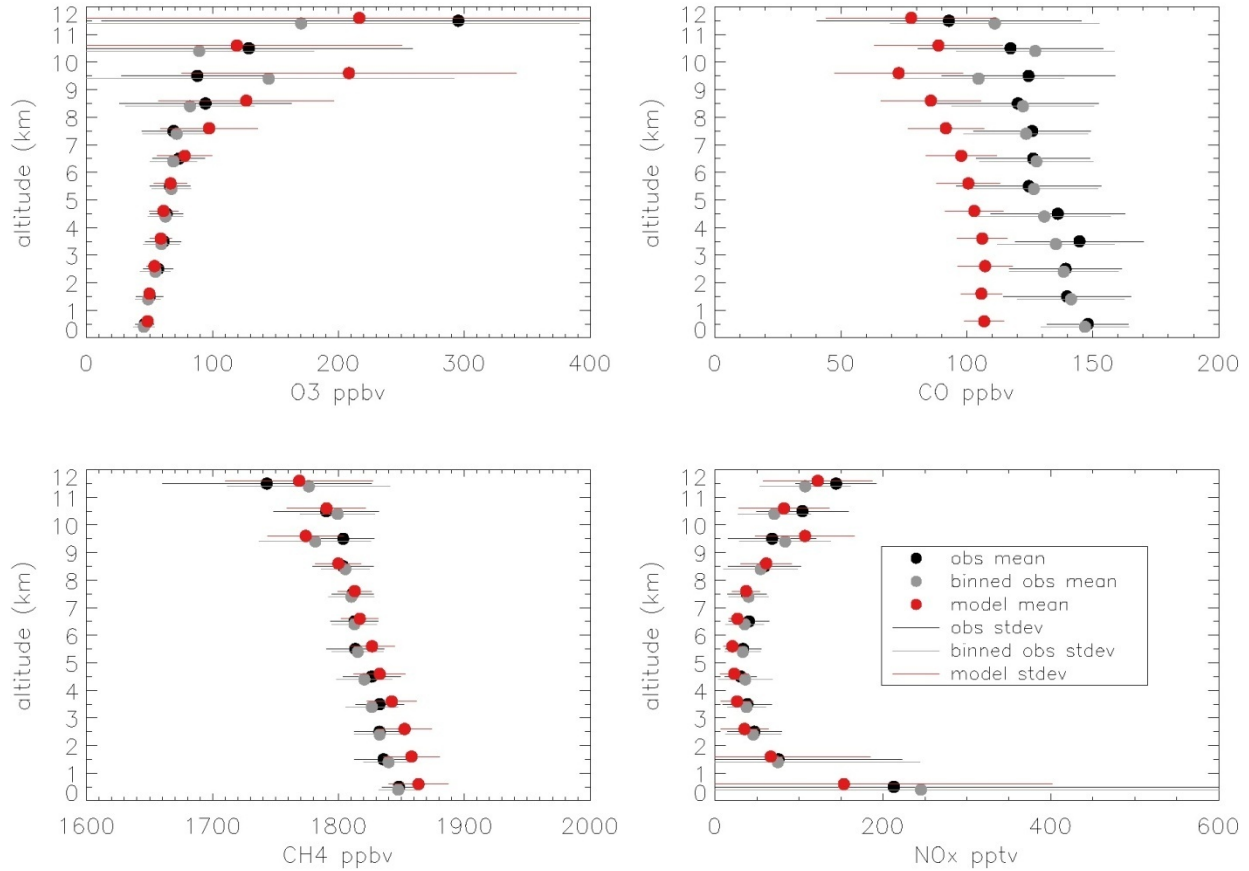


Figure 4. Vertical profiles of ozone, CO, methane, and NO_x from the Pacific phase of the INTEX-B campaign compared to the 2x2.5 degree resolution model. The DC8 aircraft observations are binned by altitude (black) and by altitude and model box (gray). Model values are sampled along the flight tracks and binned by altitude (red).

at both resolutions. Overall, resolution does not appear to be the main source of error in the 2x2.5 degree simulation.

IV. Time-dependent simulation with the free-running GCM

This section describes a time-dependent simulation from 2001-2004. The model version for this experiment is Fortuna version 2_1, running as a free GCM at 2x2.5 degree resolution. The simulation began in Dec. 2000, using restart files from the GCM ensemble run described in section II using emissions for the year 2000. This experiment included aerosols from the GOCART model coupled to the GMI chemistry. Thus aerosol concentrations for the radiation calculation and chemistry come from the GOCART model, and the GOCART model receives oxidant fields calculated by the GMI chemistry.

Emissions for the simulation were year-specific and thus varied over the course of the run. The trace gas emissions are described in section II of this report. Ship emissions of NO_x were

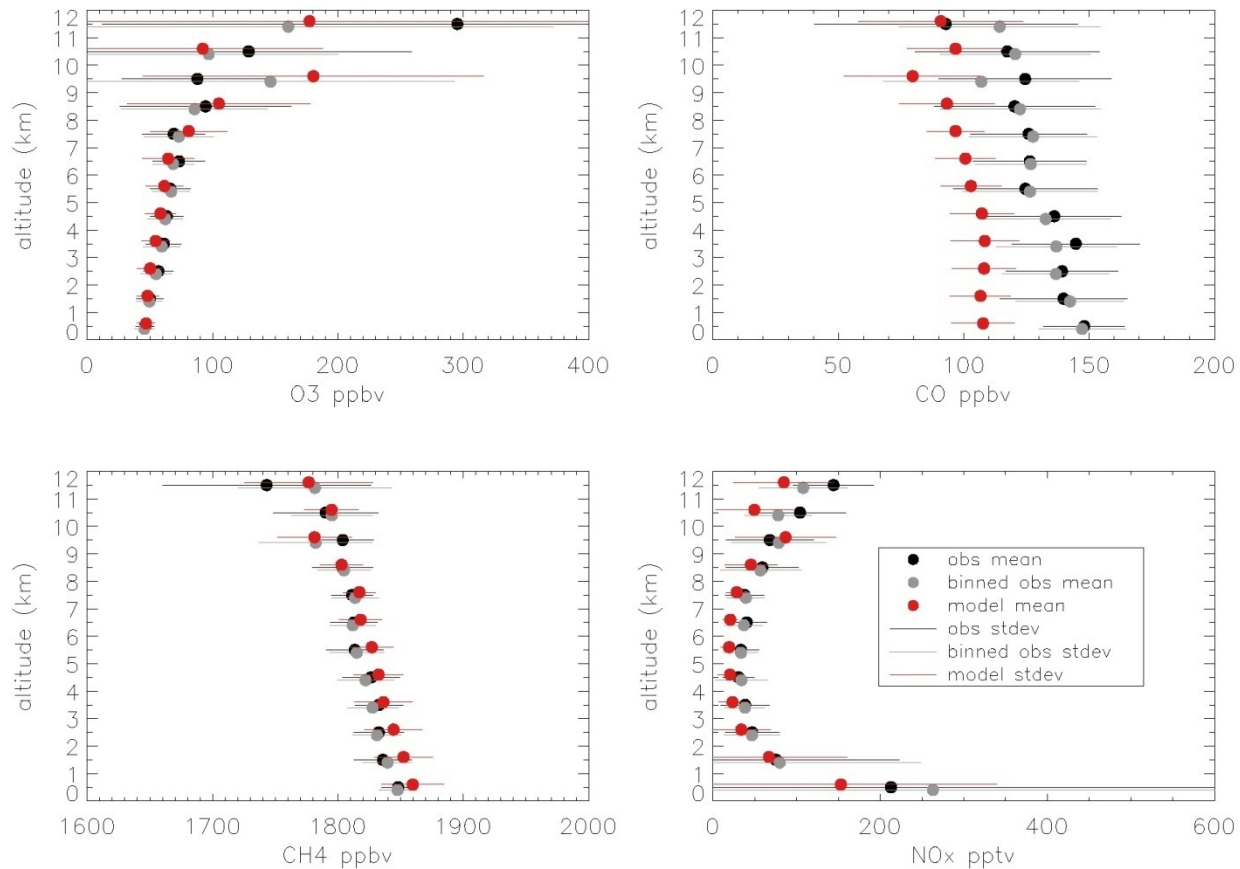


Figure 5. Same as Figure 4, but with the 1x1.25 degree resolution model.

excluded to prevent excessive ozone production over the ocean.

We present a comparison of the time-dependent free-running GCM simulation to observations below. Since the chemical and aerosol boundary conditions as well as the sea surface temperature are year-specific, the simulation incorporates some drivers of inter-annual variability. However, the free-running GCM does not produce the specific transport patterns or daily variability of the given year since the meteorology is not constrained by observations. Consequently, we focus on the model's ability to represent the monthly mean values and large-scale features of the observations.

Surface CO

The NOAA GMD network measures CO and other constituents at ground-based sites in remote locations around the globe. We compare the model to the GMD CO flask measurements (*Novelli and Masarie, 2009*) to constrain the latitudinal and seasonal variability of CO in the lower troposphere.

Figure 6 compares the monthly means of the model to GMD observations for January and July of 2004. The correlation is strong in January, with the model explaining 75% of the spatial

variability in the observations. The positive model bias is due primarily to several points in North America, pointing to a possible overestimate in emissions in the mid-west United States. The latitudinal gradient is reasonably well captured, although there is a slight high bias near the South Pole.

In July, the model correlation drops to $r^2 = 0.28$, and the slope of the regression line is drops to 0.61. The positive bias in North America and the southern hemisphere is still present. In addition, there is excessive outflow of biomass burning emissions over the equatorial oceans. This may be due in part to the lack of year-specific meteorology.

Figure 7 compares the season cycle of the model simulation for 2003 to multiple years of GMD data for 6 sites. The six sites were selected to illustrate model performance at different latitudes. At the high latitude Svalbard site, the model captures the seasonal cycle well, with a spring maximum and summer minimum. At many stations, including Svalbard, observed CO

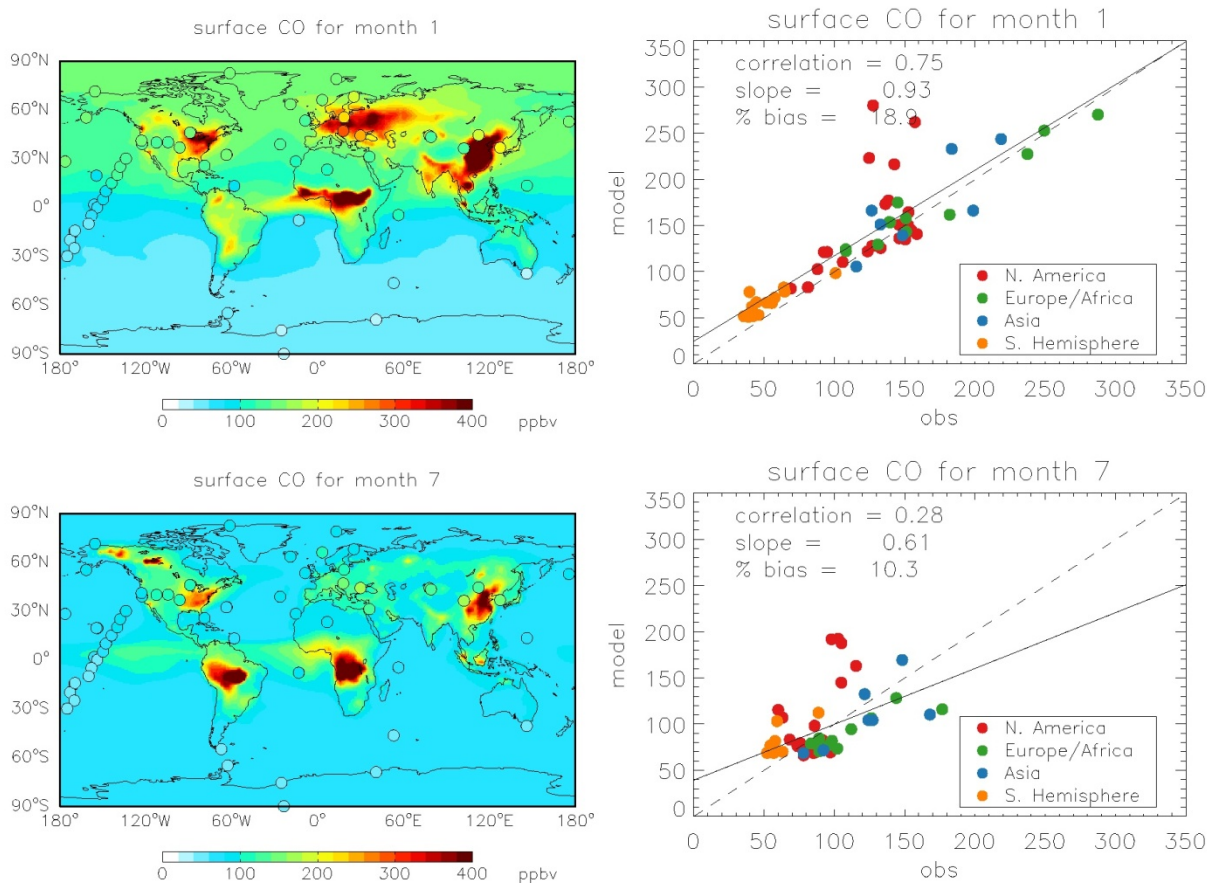


Figure 6. Left: Model surface CO overlaid with GMD observations for January (top) and July (bottom) of 2004. Right: Scatter plot of model CO sampled at the GMD observation sites against observed CO for January (top) and July (bottom). Points are color-coded by region. The regression line (solid) and 1-1 line (dashed) are also shown.

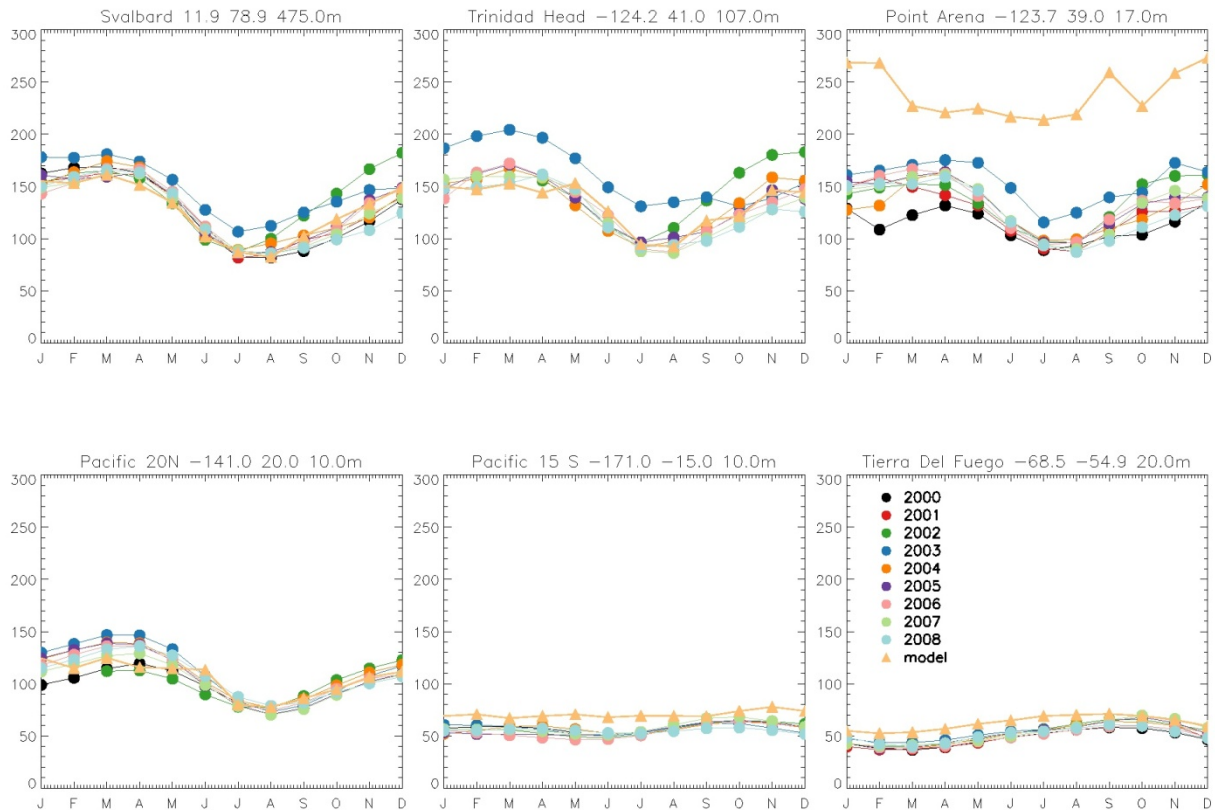


Figure 7. Seasonal cycle of surface CO in the model for 2003 (orange triangles) compared to GMD data from 2000-2008 for 6 sites.

concentrations in 2003 (blue circles) were higher than the other years. The model CO for 2003 looks more like a typical year than like the 2003 observations.

In the northern midlatitudes, model performance varies greatly from site to site. Figure 7 shows two sites in California, Trinidad Head and Point Arena, that are located with a few degrees of each other. The model captures most of the seasonal cycle well at Trinidad Head, but shows a large positive bias throughout the year at Point Arena. This is likely due to the model's inability to resolve the urban-rural gradient between the San Francisco and Point Arena.

In the tropical Pacific, the model lies within the observed variability throughout the year at 20 degrees N. At 15 degrees S, the model has a positive bias. This bias is also present at Tierra Del Fuego in the southern extratropics.

Surface Ozone over the United States

This section compares the model's surface ozone concentrations to observations from the U.S. Environmental Protection Agency's Clean Air Status and Trends Network (CASTNet). CASTNet sites (USEPA, 2007) are located in rural areas of the United States. Given the large number of

CASTNet sites, we use only the sites identified by *Reidmiller et al. (2009)* as regionally representative for comparison with the model.

Scatter plots of model vs. CASTNet monthly mean ozone for four seasons of 2003 are shown in figure 8. Only the regionally representative sites are shown. The model performs best in winter, explaining 59% of the variability. In summer and autumn, the model is biased high compared to observations at many of the sites. This is consistent with the overestimate of CO over the U.S. The comparison would likely be improved by constraining the model's meteorology to the given year.

Tropospheric NO₂ column

Figure 9 shows a comparison of the model's tropospheric NO₂ column in September 2004 with the OMI DPGC NO₂ product (*Lamsal et al., 2010*) for September 2005. Both the model and OMI show enhanced NO₂ over source regions in the Europe, East Asia, and the eastern United States. The enhancement in the eastern U.S. extends further south in OMI compared to the model, and OMI shows larger enhancements in South America and southern Africa. These

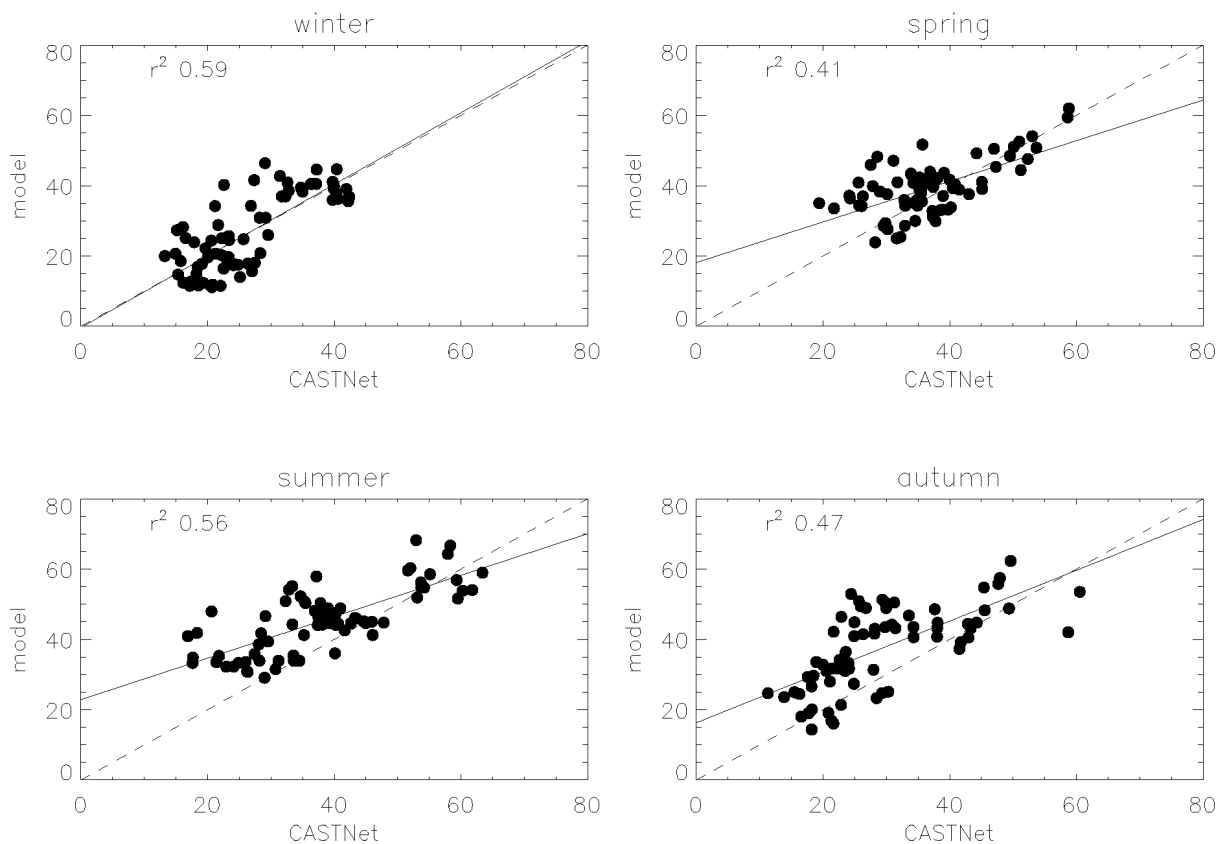


Figure 8. Model ozone versus CASTNET observations for 2003, in ppbv. Comparisons are for winter (DJF), spring (MAM), summer (JJA), and autumn (SON). The regression line (solid) and one-one line (dashed) are also shown.

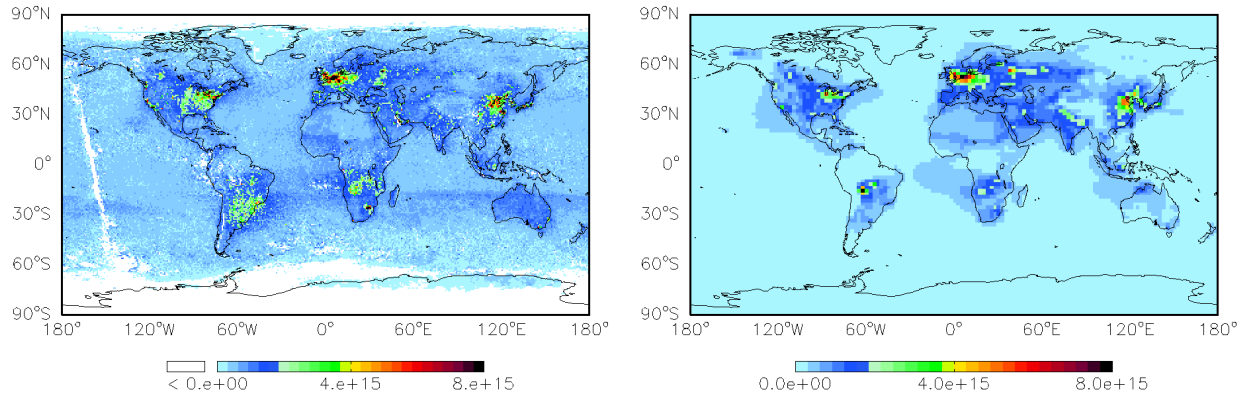


Figure 9. Tropospheric NO₂ column from OMI (left) and the model (right) for September. White values indicate missing data.

differences exceed the uncertainty in the OMI DPGC product and could indicate an underestimate in NO_x emissions in these regions.

CO comparison to MOPITT

We compare the monthly mean model CO with the MOPITT version 4 level 3 satellite product, obtained from <http://l0dup05.larc.nasa.gov/opendap/MOPITT/>, for the 500 mb level. We apply the MOPITT averaging kernels and a priori to the model CO column to give a consistent comparison with the satellite product (Deeter, 2009). In April 2002, the model underestimates the MOPITT CO in the Northern Hemisphere (Figure 10). This is consistent with the results of Shindell *et al.* (2006), who showed that a multi-model mean underestimates MOPITT CO in the northern hemisphere. The model overestimates CO in the southern hemisphere and in the equatorial biomass burning regions. This is consistent with the comparison to surface observations (Figs. 3, 6, and 7). Excessive outflow from biomass burning is also visible in September (Figure 11). Inadequate representation of the Andes at 2x2.5 degree resolution may

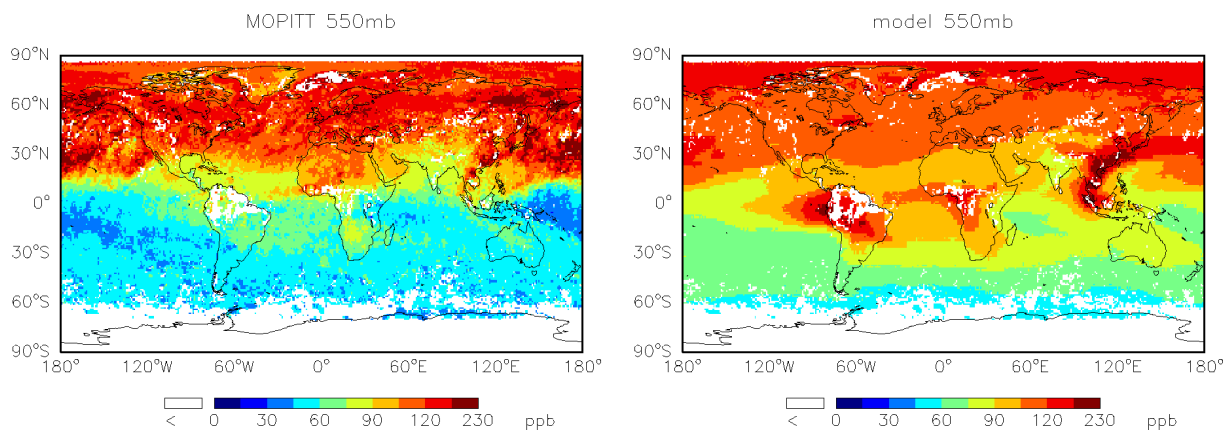


Figure 10. April CO concentrations at the 550 mb level for MOPITT (left) and the model (right). White indicates missing data.

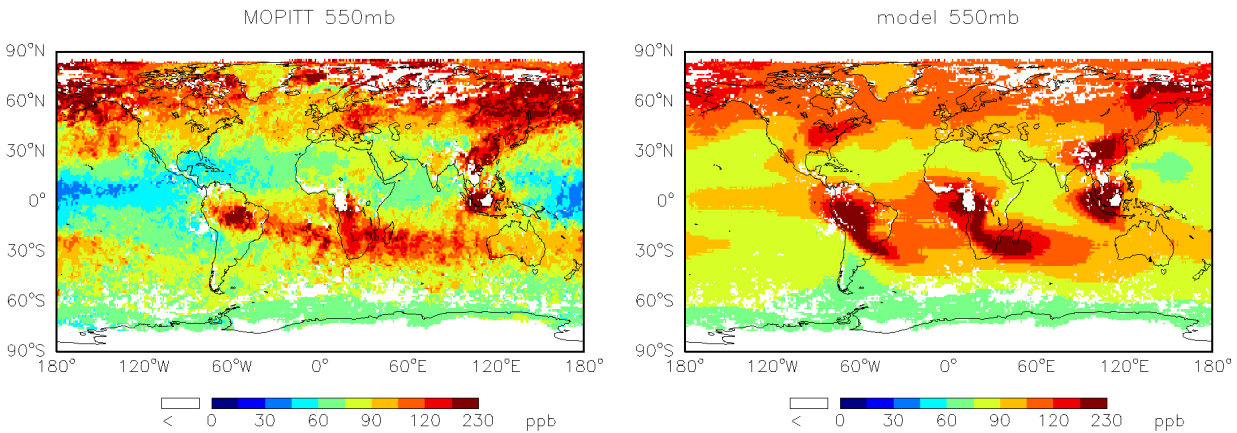


Figure 11. September CO concentrations at the 550 mb level for MOPITT (left) and the model (right). White indicates missing data.

contribute to the excessive model outflow from South America into the equatorial Pacific.

In September, the model underestimate of MOPITT CO in the high northern latitudes is less severe, but the model fails to capture the low CO in the equatorial Pacific (Figure 11). Qualitatively, the model reproduces the observed peaks in CO above the South American, African, and Indonesian biomass burning regions, as well as the eastward transport of the South American and African biomass burning CO. However, the model spreads these features over a larger area.

V. Replay to MERRA analysis

Constraining the model with the analyzed meteorological fields from MERRA has the potential to improve the distributions and variability of trace gases. The comparison between model and observations should improve since model tracers could be sampled in the same air mass as the observations. We are in the process of conducting a simulation with the configuration described in section IV, but replaying to the MERRA analysis rather than running as a GCM. This is an intermittent replay, in which the model wind and temperature fields are overwritten with the analysis every 6 hours.

Several issues were encountered during the initial replay attempt. The ozone maximum in the stratosphere initially increased relative to both the free-running GCM and a previous simulation that used the MERRA model replayed to the MERRA analysis, while ozone in the lower stratosphere decreased. Later in the simulation, concentrations of ozone and other tracers decreased rapidly to unrealistic values throughout the atmosphere.

We are currently testing a modified version of the model in a new replay run. This version changes the treatment of tracer mass following the introduction of the analyzed fields. Preliminary results suggest that this version is more consistent with the free-running GCM.

Figure 12 shows the vertical profile of ozone in the stratosphere for December 2001 in the free-running GCM, the initial replay, and the new replay. The ozone maximum in the new replay is similar to that of the GCM. In both the new replay and the GCM, ozone concentration increases gradually with height starting at level 39, whereas concentrations in the initial replay did not increase until level 33. Additional testing is under way to determine whether the new replay will maintain realistic tracer concentrations through more years of simulation.

VI. Summary

We have achieved several important steps toward consistent MERRA – trace gas distributions. The updated emissions make it possible to conduct multi-year GEOS5 simulations with emissions varying over time, allowing the model to simulate an important driver of inter-annual variability. Comparing ensembles of GCM simulations based on 2005 versus 2000 emissions indicates that the year specific emissions impact the distribution of tropospheric ozone and its precursors, with opposite effects over the United States and East Asia.

Increasing model resolution from 2x2.5 degrees to 1x1.25 degrees appears to have only a small impact on monthly mean tropospheric trace gas distributions in the GCM. However, the impact

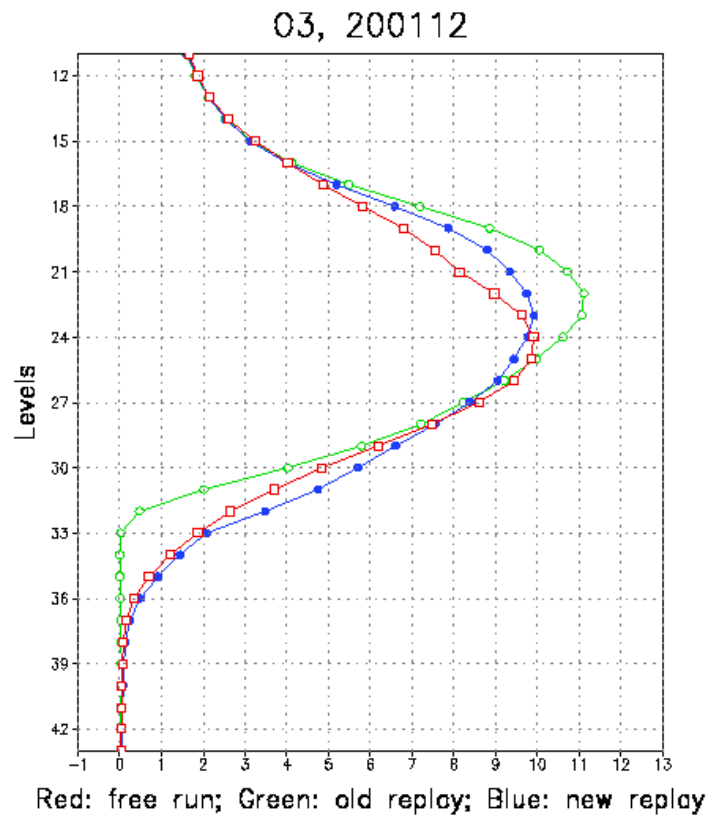


Figure 12. Comparison of the ozone profiles in the free-running GCM (red), initial replay simulation (green), and the new replay simulation (blue) as a function of model level.

might be larger if the model was replayed to the observed meteorology and compared to observations at higher time resolution.

We validated the free-running GCM simulation against surface, aircraft, and satellite observations with a focus on CO, NO_x, and ozone. This simulation, which uses the Fortuna model and updated emissions, leads to reasonable distributions of these trace gases. The ozone vertical profile compares well against aircraft observations over the Pacific from INTEX-B, and the model reproduces the seasonal cycle of CO at many of the NOAA GMD sites. Several opportunities for future improvements are also evident, such as the overestimate of CO over the United States and downwind of the South American biomass burning region.

VII. References

BRAVO: Big Bend Regional Aerosol and Visibility Observational (BRAVO) Study Emissions Inventory, H. Kuhns, M. Green, and V. Etyemezian, 2003.

CAC: http://www.ec.gc.ca/pdb/cac/cac_home_e.cfm

Charlton-Perez, C.L., M.J. Evans, J.H. Marsham, and J.G. Esler, The impact of resolution on ship plume simulations with NO_x chemistry, *Atmos. Chem. Phys.*, 9, 7505-7518, 2009.

Deeter, M.N. (2009), MOPITT (Measurements of Pollution in the Troposphere) Validated Version 4 Product User's Guide.

Duncan, B.N., S.E. Strahan, Y. Yoshida, S.D. Steenrod, and N. Livesey, Model Study of the Cross-Tropopause Transport of Biomass Burning Pollution, *Atmos. Chem. Phys.*, 7, 3713-3736, 2007a.

Duncan, B. N., J. A. Logan, I. Bey, I. A. Megretskaia, R. M. Yantosca, P. C. Novelli, N. B. Jones, and C. P. Rinsland, The global budget of CO, 1988-1997: source estimates and validation with a global model, *J. Geophys. Res.*, 112, D22301, doi:10.1029/2007JD008459, 2007b.

EMEP: <http://www.emep.int/>

EPA/NEI: <http://www.epa.gov/air/data/neidb.html>

Guenther, A., et al., A global model of natural volatile organic compound emissions, *J. Geophys. Res.*, 100, 8873-8892, 1995.

Guenther, A., B. Baugh, G. Brasseur, J. Greenberg, P. Harley, L. Klinger, D. Serca, and L. Vierling, Isoprene emission estimates and uncertainties for the Central African EXPRESSO study domain, *J. Geophys. Res.*, 104, 30,625-30,639, 1999.

Guenther, A., and C. Wiedinmyer, User's guide to Model of Emissions of Gases and Aerosols from Nature. <http://cdp.ucar.edu>. (Nov. 3, 2004)

Lamsal, L.N., R.V. Martin, A. van Donkelaar, E.A. Celarier, E.J. Bucsela, K.F. Boersma, R. Dirksen, and Y. Wang, Indirect validation of tropospheric nitrogen dioxide retrieved from the OMI

satellite instrument: Insight into the seasonal variation of nitrogen oxides at northern midlatitudes, *J. Geophys. Res.*, 115(D05392), 2009JD013351, 2010.

Novelli, P.C. and K.A. Masarie, Atmospheric Carbon Monoxide Dry Air Mole Fractions from the NOAA ESRL Carbon Cycle Cooperative Global Air Sampling Network, 1988-2008, Version: 2009-07-28, Path: <ftp://ftp.cmdl.noaa.gov/ccg/co/flask/event/>.

Randerson, J. T., G. R. van der Werf, L. Giglio, G. J. Collatz, and P. S. Kasibhatla, Global Fire Emissions Database, Version 2 (GFEDv2.1), Data set, Available on-line from Oak Ridge National Laboratory.

Reidmiller, D.R., A.M. Fiore, D.A. Jaffe, D. Bergmann, C. Cuvelier, F.J. Dentener, B.N. Duncan, G. Folberth, M. Gauss, S. Gong, P. Hess, J.E. Jonson, T. Keating, A. Lupu, E. Marmer, R. Park, M.G. Schultz, D.T. Shindell, S. Szopa, M.G. Vivanco, O. Wild, and A. Zuber, The influence of foreign vs. North American emissions on surface ozone in the US, *Atmos. Chem. Phys.*, 9, 5027-5042, 2009.

Rienecker, M.M., M.J. Suarez, R. Todling, J. Bacmeister, L. Takacs, H.-C. Liu, W. Gu, M. Sienkiewicz, R.D. Koster, R. Gelaro, I. Stajner, and J.E. Nielsen. The GEOS-5 Data Assimilation System - Documentation of Versions 5.0.1, 5.1.0, and 5.2.0. Technical Report Series on Global Modeling and Data Assimilation, 27, 2008.

Shindell, D.T. et al (2006), Multimodel simulations of carbon monoxide: Comparison with observations and projected near-future changes, *J. Geophys. Res.*, 111(D19306), 2006JD007100.

Singh, H.B., W.B. Brune, J.H. Crawford, F. Flocke, and D.J. Jacob, Chemistry and transport of pollution over the Gulf of Mexico and the Pacific: spring 2006 INTEX-B campaign overview and first results, *Atmos. Chem. Phys.*, 9, 2301-2318, 2009.

Strahan, S.E., B.N. Duncan and P. Hoor, Observationally-derived diagnostics of transport in the lowermost stratosphere and their application to the GMI chemistry transport model, *Atmos. Chem. Phys.*, 7, 2435-2445, 2007.

Streets, D.G., T.C. Bond, G.R. Carmichael, S.D. Fernandes, Q. Fu, Z. Klimont, S.M. Nelson, N.Y. Tsai, M.Q. Wang, J-H. Woo, and K.F. Yarber, An inventory of gaseous and primary aerosol emissions in Asia in the year 2000, *J. Geophys. Res.*, 108, D21, doi:10.1029/2002JD003093, 2003.

Streets, D.G, Q. Zhang, L. Wang, K. He, J. Hao, Y. Wu, Y. Tang, and G.C. Carmichael, Revisiting China's CO emissions after the Transport and Chemical Evolution over the Pacific (TRACE-P) mission: Synthesis of inventories, atmospheric modeling, and observations, *J. Geophys. Res.*, 111, D14306, doi:10.1029/2006JD007118, 2006.

Van der Werf, G. R., J. T. Randerson, L. Giglio, G. J. Collatz, and P. S. Kasibhatla, Interannual variability in global biomass burning emission from 1997 to 2004, *Atmospheric Chemistry and Physics*, 6, 3423-3441, 2006.

van Donkelaar, A., R. V. Martin, W. R. Leitch, A.M. Macdonald, T. W. Walker, D. G. Streets, Q. Zhang, E. J. Dunlea, J. L. Jimenez, J. E. Dibb, L. G. Huey, R. Weber, and M. O. Andreae, Analysis of Aircraft and Satellite Measurements from the Intercontinental Chemical Transport Experiment (INTEX-B) to Quantify Long-Range Transport of East Asian Sulfur to Canada, *Atmos. Chem. Phys.*, 8, 2999-3014, 2008.

VISTAS: <http://www.vistas-sesarm.org/index.asp>

Wang, Y., D. J. Jacob, and J. A. Logan, Global simulation of tropospheric O₃-NO_x-hydrocarbon chemistry, 1. Model formulation, *JGR*, 103/D9, 10,713-10,726, 1998.

Yevich, R. and J.A. Logan, An assessment of biofuel use and burning of agricultural waste in the developing world, *Glob. Biogeochem. Cycles*, 17(4), 2003.

US Environmental Protection Agency (2007), Clean Air Status and Trends Network (CASTNet) factsheet, available at: http://www.epa.gov/castnet/docs/CASTNET_factsheet_2007.pdf

Zhang, Q., D.G. Streets, G.R. Carmichael, K.B. He, H. Huo, A. Kannari, Z. Klimont, I.S. Park, S. Reddy, J.S. Fu, D. Chen, L. Duan, Y. Lei, L.T. Wang, and Z.L. Yao, Asian emissions in 2006 for the NASA INTEX-B mission, *Atmos. Chem. Phys.*, 9, 5131-5153, 2009.